

---

## Self-Interference Patterns and Their Application to Target Characterization

The uniformity requirements of direct-drive targets are stringent. The requirements on both sphericity and wall thickness uniformity are of the order of less than 1%. In the past, dual-beam interference microscopy has been used at LLE to characterize the wall thickness and uniformity of transparent targets.<sup>1</sup> With this technique, an interference pattern is formed between one beam that passes through the target and a second beam, split off from the first, that passes around the target. By comparison with computer-generated templates, these interference patterns can yield the wall thickness and its uniformity to a high degree of accuracy.<sup>2</sup>

This article describes an alternative interferometric technique that is simpler to use and that provides a rapid characterization of both the wall thickness and the uniformity of single-shell targets. These are typically polystyrene (CH) shells, which are selected prior to being coated with layers of various materials and/or filled with D<sub>2</sub>, DT, or some other desired gas. These shells have the remarkable property that, when irradiated with a spatially incoherent, narrow-bandwidth light source and viewed using only a compound microscope, they display self-interference patterns (SIP's) such as the one shown in Fig. 64.31. These patterns are distinct concentric fringes when the target is uniform, but faint, distorted, or discontinuous fringes form when the target is nonuniform. Previously, SIP's have not been used because they are clearly observed only in targets of very high quality, with uniformity typically better than 1%.

This technique is currently being used for the preliminary selection of polystyrene shells typically of 800- to 1000- $\mu\text{m}$  diameter and 5- to 12- $\mu\text{m}$  wall thickness. The fringe locations have been modeled using ray tracing and agree well with actual measurements of well-characterized shells. Shells can be selected with the wall thickness known to  $\pm 0.5 \mu\text{m}$  and with uniformity better than  $0.05 \mu\text{m}$ .

### Origin of the Self-Interference Pattern

SIP formation results from multiple reflections of rays within the shell walls. The three relevant beam paths are

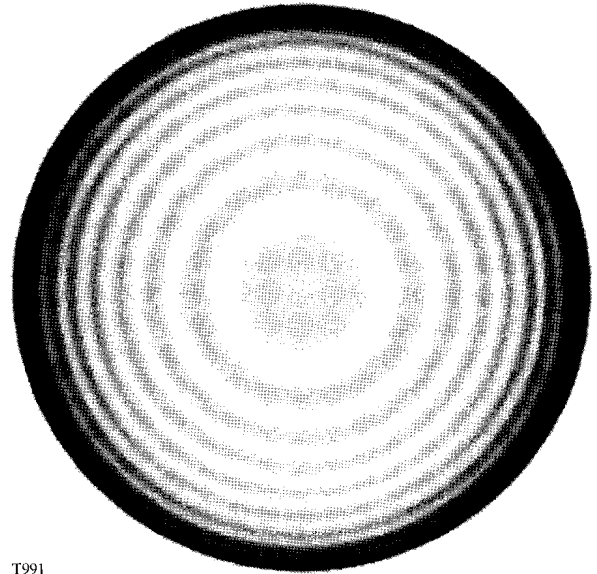


Figure 64.31  
A compound-microscope image of a self-interference pattern produced by a symmetric capsule when illuminated with narrow-bandwidth light. The polystyrene (CH) capsule has an 850- $\mu\text{m}$  diameter and a 7- $\mu\text{m}$  thickness.

illustrated in Fig. 64.32. Beam 1 passes straight through the shell, beam 2 undergoes two reflections on the input side, and beam 3 undergoes two reflections on the output side. For a perfect shell, the emerging wavefronts of beams 2 and 3 are virtually identical, so they combine coherently and interfere with the wavefront of beam 1 to form the SIP. For an imperfect shell, in which the input and output thicknesses are different, a single SIP is not formed, but one observes a combination of two SIP's, one corresponding to the input side, (beams 1 and 2 interfering) and the other to the output side (beams 1 and 3).

In Fig. 64.32, all rays are shown backprojected (with dashed lines) to the point on the object plane ( $z = 0$ ) from which they appear to come. Exact ray-tracing calculations show that a ray incident at a height  $r_i$  appears to come from a height  $r_a$  in the object plane where the difference between  $r_i$  and  $r_a$  is negligi-

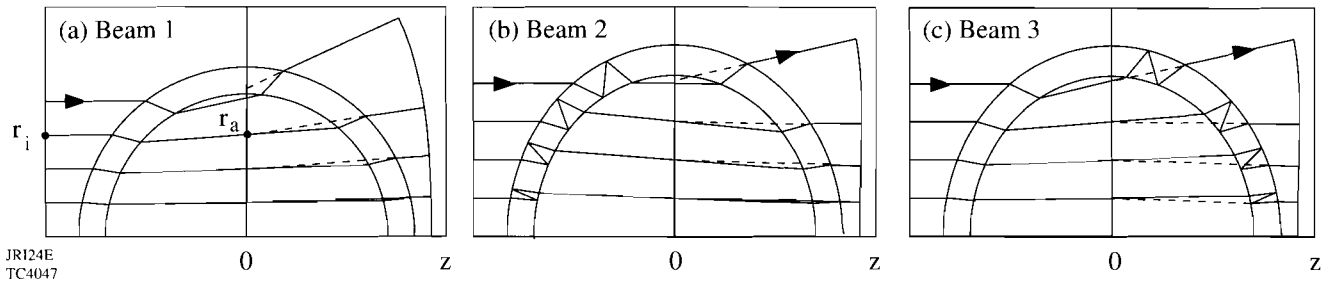


Figure 64.32

Ray paths through the target of (a) beam 1, (b) beam 2, and (c) beam 3. In each case the rays enter from the left, the emerging wavefront is drawn on the right, and the emerging rays are backprojected (dashed lines) to their apparent origin in the object plane ( $z = 0$ ). For a perfect target, wavefronts 2 and 3 are virtually identical, add coherently, and form the self-interference pattern (SIP) through combination with wavefront 1.

bly small (typically less than  $0.1 \mu\text{m}$  except very close to the edge of the target) for each of the three beam paths. This is true only for the object plane  $z = 0$ . Since the source is spatially incoherent, two rays can interfere only if they originate from the same incident ray. Thus, the only object plane that permits the SIP formation is the midplane  $z = 0$ . In this sense the fringes can be described as being localized in this plane. In contrast, if the illumination was spatially coherent as in the dual-beam interferometry technique described in Ref. 2, interference fringes could be obtained for any object plane.

For a spherically symmetric target, the locations of the interference fringes may be calculated by plotting the optical path difference  $\text{OPD}_2 - \text{OPD}_1$  between beams 2 and 1 as a function of apparent radius  $r_a$  in the object plane (see Fig. 64.33). [ $\text{OPD}_i$  is defined as the optical path difference (in

centimeters) between a ray of beam  $i$  ( $i = 1-3$ ) and a reference ray passing through vacuum, but in Fig. 64.33 it is plotted in waves.] In this example, six bright fringes will be seen with optical path differences ranging from 29 to 24 waves, and the loci of greatest intensity in an interferogram can be simply constructed by drawing circles at the corresponding radii. For targets with nonuniformities in the  $(x,y)$  plane, i.e., targets that are not rotationally symmetric about the  $z$  axis, interferograms can be formed by tracing a grid of rays through the target and drawing a contour plot of the optical path difference with the contour levels chosen to be integer numbers of waves.<sup>3</sup>

In place of Fig. 64.33, the “universal curves” of Fig. 64.34 can be used to predict the behavior of all perfectly uniform targets of interest. In this figure, the optical path differences  $\text{OPD}_1$  and  $\text{OPD}_2$ , and the difference  $\text{OPD}_2 - \text{OPD}_1$ , are all

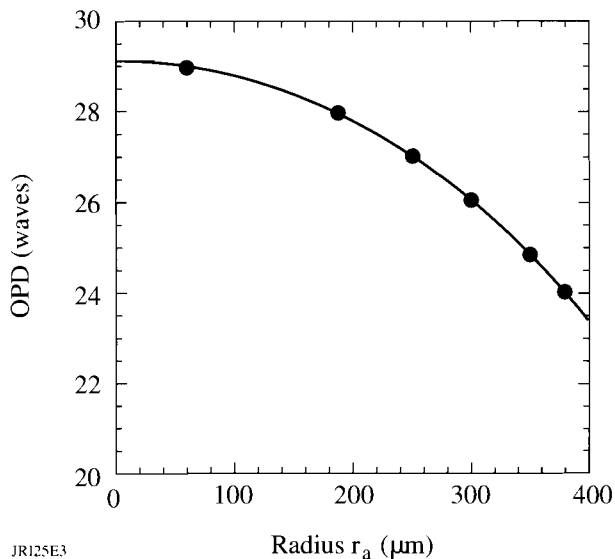
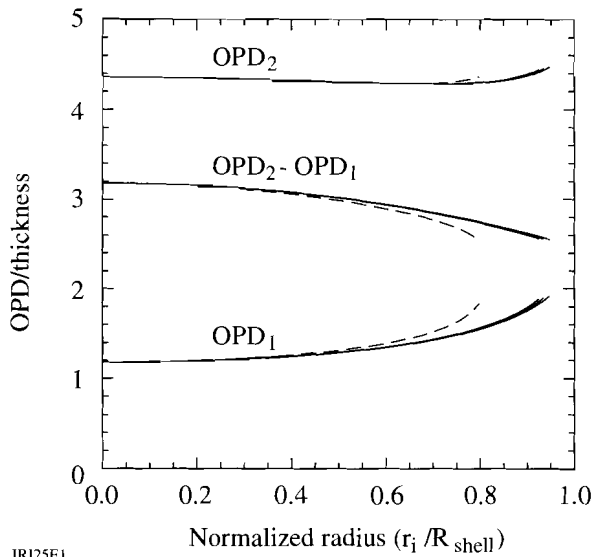


Figure 64.33

The optical path difference ( $\text{OPD}_2 - \text{OPD}_1$ ) between beam 2 and beam 1 for a representative CH target with an  $850\text{-}\mu\text{m}$  outer diameter, a  $5\text{-}\mu\text{m}$  thickness, and a refractive index at  $546 \text{ nm}$  of  $1.59$ . The abscissa is the apparent radius  $r_a$  in the object plane (see Fig. 64.32), which is almost identical to the incident radius  $r_i$ . The solid points correspond to integer values of optical path difference and thus give the radii of the centers of the bright fringes.

JR125E3  
TC4048



JRI25E1  
TC4049

Figure 64.34

Universal curves governing the formation of the self-interference pattern. By plotting the OPD divided by the shell thickness  $t$  on the vertical axis and the normalized radius ( $r_i/R_{\text{shell}}$ ) on the horizontal axis, the three quantities  $OPD_1/t$ ,  $OPD_2/t$ , and  $OPD_2 - OPD_1/t$  are virtually independent of shell diameter and thickness. The curves shown here are for four shells with outer diameters ranging from 250 to 1500  $\mu\text{m}$  and thicknesses ranging from 2 to 20  $\mu\text{m}$ . The dashed curves correspond to a 250- $\mu\text{m}$  diameter and a 20- $\mu\text{m}$  thickness.

plotted against the normalized radius  $r_i/R_{\text{shell}}$ , where  $R_{\text{shell}}$  is the average of the inner and outer shell radii. (Similar results are obtained by normalizing to either the inner or the outer radius.) Graphs are superposed for CH targets with outer diameter  $d = 250$  to 1500  $\mu\text{m}$  and thickness  $t = 2$  to 20  $\mu\text{m}$ ; specifically, the four extreme combinations are included. All curves are virtually identical except for the low-aspect-ratio combination ( $d = 250 \mu\text{m}$ ,  $t = 20 \mu\text{m}$ ), which is not of current interest for experiments on OMEGA.

The values of OPD for rays passing through the center of a perfect target with respect to parallel rays passing external to the target are given by

$$OPD_1 = 2t(n - 1), \quad (1)$$

$$OPD_2 = OPD_3 = 4tn - 2t, \quad (2)$$

$$OPD_2 - OPD_1 = 2tn. \quad (3)$$

For example, for  $n = 1.59$  and a wavelength  $\lambda = 546 \text{ nm}$ , as used throughout this article, the difference in  $(OPD_2 - OPD_1)/t$  between the center and the edge is  $\Delta(OPD_2 - OPD_1)/t = 0.62$ . (The edge is understood to correspond to 95% of the inner-shell radius, i.e., approaching the last ray that will be transmitted through the target.) Thus, if  $N$  bright fringes are counted,  $\Delta(OPD_2 - OPD_1) \approx N \lambda$  and

$$t \approx N\lambda/0.62 = 0.88 N \mu\text{m}. \quad (4)$$

The accuracy of Eq. (4) is limited by the accuracy with which  $\Delta(OPD_2 - OPD_1)$  can be estimated by counting fringes. The method will work as long as the time difference between interfering rays [ $(OPD_2 - OPD_1)/c$ , where  $c$  is the speed of light] is less than the coherence time of the source. For the low-pressure mercury vapor source<sup>4</sup> used in the work reported here, this criterion is satisfied for wall thicknesses  $t \leq 15 \mu\text{m}$ .

Ray trajectories have been calculated using both exact ray tracing and a paraxial approximation that includes third-order spherical aberration. The paraxial approximation does not accurately predict the wavefront near the edge of the target, where higher-order spherical aberration is present. However, the error incurred is approximately equal in each of wavefronts 1, 2, and 3. Thus,  $\Delta(OPD_2 - OPD_1)$  and  $\Delta(OPD_3 - OPD_1)$  are nearly identical for the paraxial and exact ray-tracing treatments, and results obtained by the two methods agree closely.

One notable property of the SIP is its sensitivity to  $t$ . For  $n = 1.59$ , the quantity detected is  $OPD_2 - OPD_1 = 3.2t$  [from Eq. (3)] compared with  $OPD_1 = 1.2t$  [from Eq. (1)] as would apply to conventional two-beam interferometry. This method is thus roughly three times more sensitive to changes in target thickness.

Another property of the SIP is that for very small differences between  $t_L$  and  $t_R$ , the thicknesses on the left and right of the target in Fig. 64.32, respectively, a single interferogram is not formed. For a half-wave difference in the OPD along the

axis, enough to destroy the SIP, the necessary thickness difference is given by

$$2t_L n - 2t_R n = 0.5 \lambda$$

or

$$t_L - t_R = 0.086 \mu m, \tag{5}$$

corresponding to a 1.2% peak-to-valley thickness variation for a typical 7- $\mu m$  shell. Targets displaying a distinct SIP have a much better uniformity than this.

Some examples of calculated SIP's are given in Figs. 64.35–64.37. Figure 64.35 shows interferograms of three targets with various wall thicknesses, from which Eq. (4) can be verified. Figure 64.35(b) matches the experimental interferogram of Fig. 64.31 very well. Figure 64.36 shows interferograms of three targets with slightly different wall thicknesses  $t$ , to show the sensitivity of the SIP to  $t$  as alluded to above. The OPD through the center changes by 0.29 waves for each 0.05- $\mu m$  change in thickness. Each change is clearly distinguishable, especially if the location of the first or second clear fringe is measured. Finally, Fig. 64.37 shows a combination of two SIP's with a 1% nonuniformity. The nonuniformity is directed along the  $z$  direction [Fig. 64.37(a)], at 45° to the  $y$  and  $z$  directions [Fig. 64.37(b)], and along the  $y$  direction [Fig. 64.37(c)]. In each case the heavy and light lines indicate

the two SIP's; in each of Fig. 64.37(a) and Fig. 64.37(b) a distinct SIP would not be seen in practice, so that the nonconcentricity would be easily detected. In Fig. 64.37(c), where the defect is aligned perpendicular to the viewing direction, an up-down shift can be observed in the calculated fringe pattern but would probably not be readily observed in practice. In Fig. 64.37(c) the two SIP's add coherently as the two thicknesses  $t_L$  and  $t_R$  are equal.

Actual target imperfections rarely match the simplified imperfections shown in Fig. 64.37. An example of an imperfect target is shown in Fig. 64.38. The fringes on the bottom are not too different from those of Fig. 64.31, but extra fringes are observed near the top where, clearly, the target contains a region of excessive thickness. There also appears to be some moiré beating in this area between the two SIP's, one of which is stronger because the microscope is focused closer to its plane of localization.

It does not require a large deviation from spherical symmetry for the two SIP's to not combine coherently. When the apparent positions  $r_a$  in the object plane of the two rays associated with beam 2 and beam 3 (see Fig. 64.32) differ by the spatial coherence length of the light source imaged onto this plane, coherence is lost. An alternative and more general approach is to consider every incident ray, including rays other

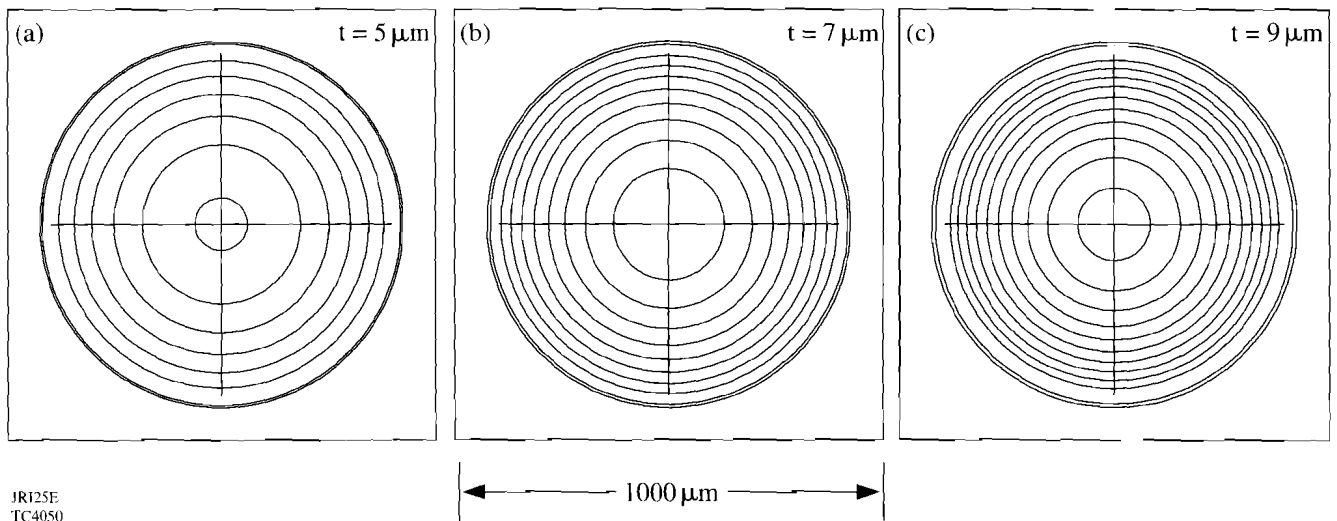
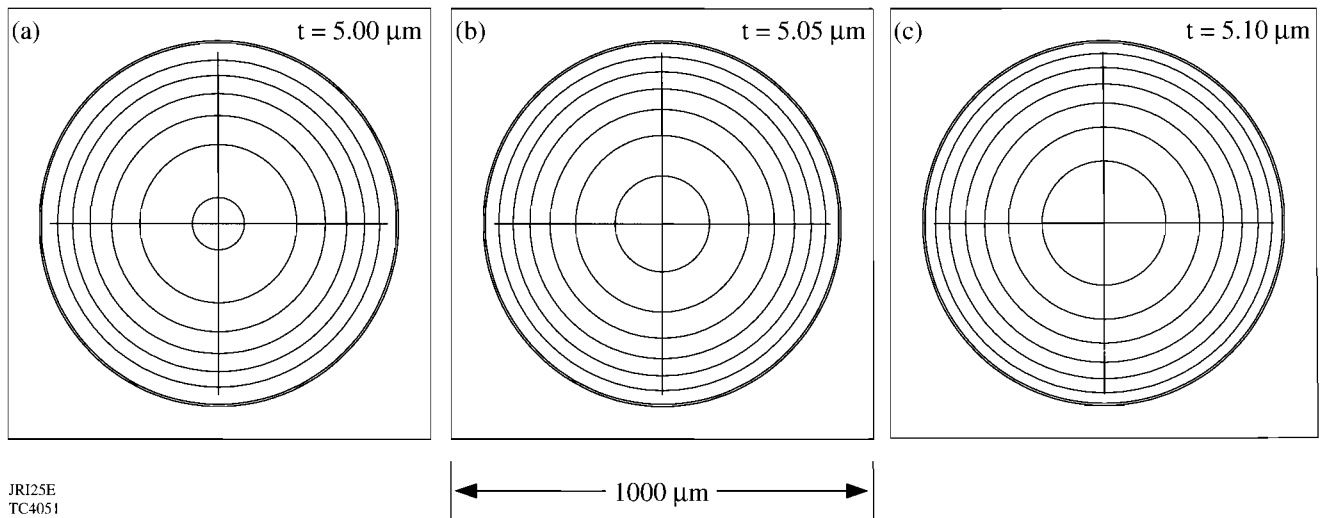


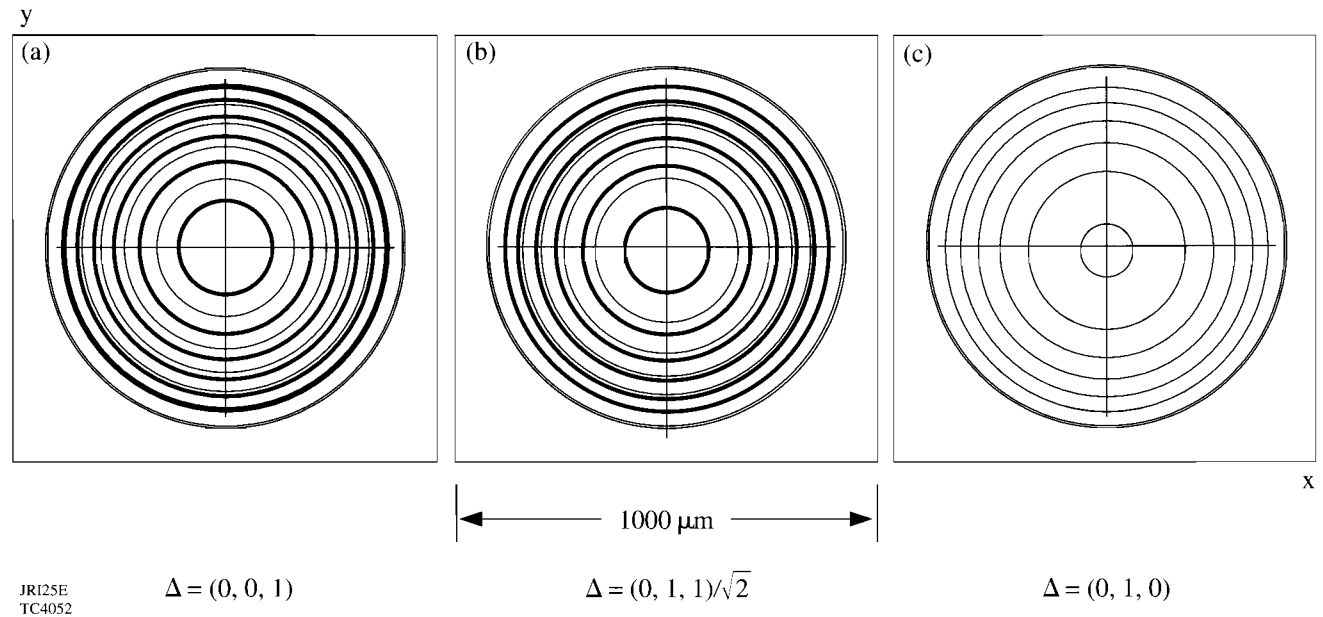
Figure 64.35  
 Calculated SIP's for three perfectly symmetric polystyrene targets, all with an outer diameter of 850  $\mu m$ , but with thicknesses  $t$  ranging from 5 to 9  $\mu m$ . The outer circles indicate the edge of the target and the other circles are interference fringes. The SIP for  $t = 5 \mu m$  corresponds to Fig. 64.33 and that for  $t = 7 \mu m$  corresponds to Fig. 64.31. The target thickness in microns can be estimated by multiplying the number of bright fringes by 0.88.



JRI25E  
TC4051

Figure 64.36

Calculated SIP's for three polystyrene targets with slightly different wall thicknesses. Thickness differences as small as  $0.05 \mu\text{m}$  can be detected if attention is paid to the location of the inner fringes.



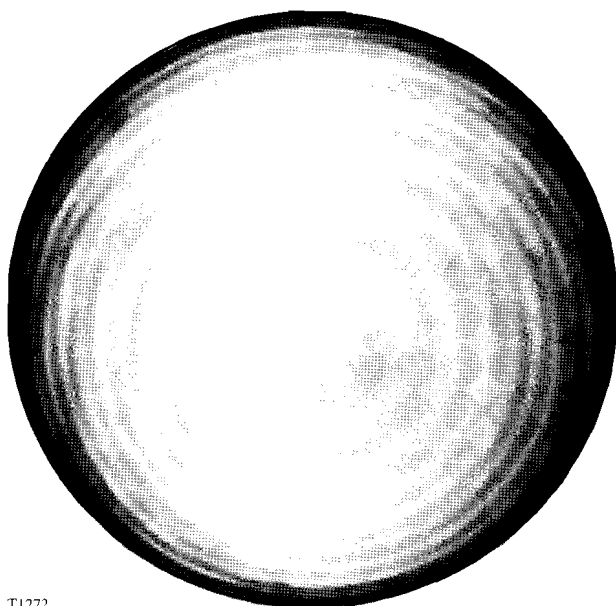
JRI25E  
TC4052

Figure 64.37

Calculated SIP's formed by interference between beams 1 and 2 (light lines) and between beams 1 and 3 (heavy lines) for a polystyrene target with a 1% thickness nonuniformity for three different orientations of the nonuniformity given by the unit vectors  $\Delta$ . (The inner surface is spherical but shifted  $0.05 \mu\text{m}$  in the direction of  $\Delta$ .) In case (a) the two SIP's are out of phase by a half-wave in the center, so that no distinct interference pattern would be seen in practice. Thus, the existence of a distinct SIP indicates a target with better than  $0.05\text{-}\mu\text{m}$  thickness uniformity.

than the parallel set shown in Fig. 64.32, as independent due to the spatially incoherent nature of the source. For each incident ray there are three emerging rays, corresponding to beam paths 1–3. Projecting their trajectories back, there will be a position where rays 1 and 2 cross for an ideal target, and a point of closest approach for a nonideal target. There will be a separate point of closest approach for rays 1 and 3. Constructive interference will occur if the backprojected rays pass sufficiently close to each other. For an ideal target, rays with different angles of incidence will cross in rotated midplanes but may still be close enough to each other in the object plane to interfere. Viewed alternatively, each angle of incidence will result in an interference pattern that appears to be formed within the target with a certain localization depth along the propagation direction; the patterns for different angles then add in intensity. This property of the system makes it unnecessary to illuminate the targets with collimated light and enhances the brightness of the images. It suffices to use a narrow-bandwidth extended source such as a low-pressure mercury-vapor lamp.

From Fig. 64.32, it is evident that the SIP is largely independent of the gas inside the target, whatever its pressure. This is because the interfering rays have a small angle and lateral



T1272

Figure 64.38  
Example of an interference pattern formed from a poor-quality shell. Two SIP's are produced, as in Fig. 64.37, but they are not concentric.

displacement relative to each other; thus, they traverse almost the same optical path through the gas. This allows the target's wall thickness to be measured, after it is pressurized with fusion fuel, without accurate knowledge of the fill pressure. This is not possible with dual-beam interferometry since the optical path through the target is relative to an equivalent path in air. In this case, the difference between the refractive index of the fill gas and that of the surrounding air must be accounted for and subtracted from the total optical path length through the target to determine its wall thickness.

**Fringe Visibility**

Uniform shells possess a relatively high fringe visibility with respect to nonuniform shells since the reflected wavefronts (beams 2 and 3) superpose both in space and phase, thereby interfering constructively to modify the amplitude of the transmitted wavefront (beam 1). Assume electric-field amplitude transmission coefficients  $T_1$  and  $T_2$  and a reflection coefficient  $R$ , respectively, at each interface. ( $T_1$  and  $T_2$  apply to rays passing from air to shell and from shell to air, respectively. Similar coefficients  $R_1$  and  $R_2$  could be defined, but they are equal in magnitude.) In practice,  $T_1$ ,  $T_2$ , and  $R$  will depend on the angle of incidence at each interface, but the assumption of single values for  $T_1$ ,  $T_2$ , and  $R$  will be good near the target center. For  $n = 1.59$ ,  $R = (n - 1)/(n + 1) = 0.228$ . Then the amplitudes of transmitted waves 1–3 are given respectively by

$$\begin{aligned}
 A_1 &= A_0 T_1^2 T_2^2, \\
 A_2 &= A_0 T_1^2 T_2^2 R^2, \\
 A_3 &= A_0 T_1^2 T_2^2 R^2.
 \end{aligned}
 \tag{6}$$

For a perfectly symmetric shell, waves 2 and 3 interfere constructively to produce a wave with amplitude

$$A_2 + A_3 = 2A_0 T_1^2 T_2^2 R^2.
 \tag{7}$$

Interference between these two waves and the purely transmitted wave 1 gives amplitudes

$$A_1 \pm (A_2 + A_3) = A_0 T_1^2 T_2^2 (1 \pm 2R^2)
 \tag{8}$$

with  $\pm$  indicating constructive (destructive) interference. The

fringe visibility is then

$$V \equiv \frac{I_{\max} - I_{\min}}{I_{\max} + I_{\min}} = \frac{(1 + 2R^2)^2 - (1 - 2R^2)^2}{(1 + 2R^2)^2 + (1 - 2R^2)^2} \quad (9)$$

$$= \frac{4R^2}{1 + 4R^4}, \quad (10)$$

where  $I_{\max}$  and  $I_{\min}$  denote maximum and minimum intensities. Without waves 2 and 3 combining, Eq. (8) would be replaced by

$$A_1 \pm A_2 = A_0 T_1^2 T_2^2 (1 \pm R^2) \quad (11)$$

for interference between waves 1 and 2, with

$$V' = \frac{2R^2}{1 + R^4}. \quad (12)$$

Thus, the visibility is greater by about a factor of 2 when waves 2 and 3 constructively interfere. For example, for  $n = 1.59$ ,  $R = (n - 1)/(n + 1) = 0.228$ ,  $V = 0.206$ , and  $V' = 0.104$ .

**Experimental Verification**

The wall thicknesses of several glass shells were measured using dual-beam interferometry with an uncertainty of  $\pm 0.05 \mu\text{m}$ . Their outside diameters were also determined using

a calibrated compound microscope to within  $\pm 3 \mu\text{m}$ . The refractive index of the glass shells was measured by fracturing shells from the same glass batch, immersing them in index-matching fluid, and varying the fluid temperature until the glass shards could not be differentiated from the fluid.<sup>5</sup> This method utilizes the temperature dependence of the refractive index of the index-matching fluid and results in a very sensitive refractive-index measurement with an uncertainty as low as  $\pm 0.0002$ . The shells were then imaged with the same compound microscope used to measure their outside diameter, but with a 10-nm-bandwidth interference filter centered on a 546-nm wavelength placed between its diffuser and condenser; this time the diameters of the SIP fringes were measured.

A comparison between the measured SIP fringe diameters and the calculated ones for a specific shell of thickness  $2.89 \pm 0.05 \mu\text{m}$  is given in Table 64.III. Calculated fringe diameters are given for  $2.89 \mu\text{m}$  and  $2.93 \mu\text{m}$ . The latter thickness, well within the uncertainty of the thickness measurement, gives the better agreement between the measured and calculated SIP fringe diameters.

The SIP fringe diameters (when normalized to the shell diameter) are much less sensitive to small errors in the outside diameter than in the wall thickness because the universal curves of Fig. 64.34 depend primarily on the ratio  $r_i/R_{\text{shell}}$ . As noted above, the SIP is more sensitive to wall thickness variations than the dual-beam interferogram of the same target. In particular, the positions of the SIP innermost fringes provide information not so readily available from dual-beam interferometry because of the problem of establishing the piston, i.e., the absolute value of the optical path through the target center.

Table 64.III: A comparison between the calculated and measured SIP fringe diameters for a glass ( $n = 1.4648 \pm 0.003$ ) shell with a  $255 \pm 3 \mu\text{m}$  outside diameter illuminated with 546-nm light with a 10-nm bandwidth. The measured wall thickness of  $2.89 \pm 0.05 \mu\text{m}$  was obtained using a Mach-Zehnder interference microscope. The SIP fringe diameters were measured with a calibrated eyepiece reticle while viewing the shell through a compound microscope. A wall thickness of  $2.93 \mu\text{m}$  gave the best agreement between the calculated and measured SIP fringe diameters and is within the uncertainty of the wall thickness measurement. (The outermost predicted fringe was not observed in the measured SIP.)

Calculated fringe diameters ( $\mu\text{m}$ )		Measured fringe diameters ( $\mu\text{m}$ )
$t = 2.89 \mu\text{m}$	$t = 2.93 \mu\text{m}$	
94	110	$112 \pm 5$
160	168	$167 \pm 3$
202	210	$206 \pm 3$
238	242	

### Conclusions

The SIP fringe technique is now routinely used to preselect targets based on their wall thickness and nonconcentricity prior to high-precision interferometric characterization. This technique requires only a compound microscope with a narrow-bandwidth interference filter or a stereo microscope and a diffuse mercury-vapor illumination source. The wall thickness is determined to within  $\pm 0.5 \mu\text{m}$  by counting the number of fringes in the SIP, independent of the outside diameter, and the thickness uniformity is verified to an accuracy better than  $0.05 \mu\text{m}$ . In addition, the wall thickness of gas-filled targets can be determined to the same accuracy without knowledge of the type of gas or its pressure.

### ACKNOWLEDGMENT

This work was supported by the U.S. Department of Energy Office of Inertial Confinement Fusion under Cooperative Agreement No. DE-FC03-92SF19460, the University of Rochester, and the New York State Energy Research and Development Authority. The support of DOE does not constitute an endorsement by DOE of the views expressed in this article.

### REFERENCES

1. G. M. Halpern *et al.*, *J. Appl. Phys.* **48**, 1223 (1977).
2. R. Q. Gram, M. D. Wittman, C. Immesoete, H. Kim, R. S. Craxton, N. Sampat, S. Swales, G. Pien, J. M. Soures, and H. Kong, *J. Vac. Sci. Technol. A* **8**, 3319 (1990).
3. M. K. Prasad, K. G. Estabrook, J. A. Harte, R. S. Craxton, R. A. Bosch, Gar. E. Busch, and J. S. Kollin, *Phys. Fluids B* **4**, 1569 (1992).
4. Green Monochromatic Lamp, Edmund Scientific Co., 101 E. Gloucester Pike, Barrington, NJ 08007-1380.
5. R. P. Cargille Laboratories, Inc., Cargille Scientific, Inc., Cedar Grove, NJ 07009.